crystals

MDPI

Article

Synthesis, Crystal Structure, Gas Absorption, and Separation Properties of a Novel Complex Based on Pr and a Three-Connected Ligand

Jie Sun [1,*], Minghui Zhang [2], Aiyun Wang [1] and Ziwei Cai [1]

[1] School of Life Science, Ludong University, Yantai 264025, China; wanay1977@126.com (A.W.); skycaiziwei@163.com (Z.C.)

[2] College of Science, China University of Petroleum (East China), Qingdao 266580, China; zhangmhupchuaxue@163.com

* Correspondence: jiesunld@163.com

Academic Editor: George E. Kostakis

Received: 29 October 2017; Accepted: 7 December 2017; Published: 11 December 2017

Abstract: A novel Pr complex, constructed from a rigid three-connected H_3TMTA and praseodymium(III) ion, has been synthesized in a mixed solvent system and characterized by X-ray single crystal diffraction, infrared spectroscopy, a thermogravimetric analysis, an element analysis, and powder X-ray diffraction, which reveals that complex **1** crystallizes in a three-dimensional porous framework. Moreover, the thermal stabilities and the fluorescent and gas adsorption and separation properties of complex **1** were investigated systematically.

Keywords: rare earth complex; solvothermal conditions; thermal stabilities; fluorescent property; gas uptake

1. Introduction

During the past few decades, a lot of effort has been devoted to the rational design and synthesis of coordination polymers (CPs) in the field of chemical and material science due to their fascinating architectures and topologies together with their potential applications [1–8]. Besides the N-containing ligands, rigid multi-carboxylate ligands are intriguing components owing to their easily predictable and stable resulting framework [9–17]. Among all of the multi-carboxylate ligands, many C_3-symmetric tricarboxylate ligands have been extensively investigated to construct CPs with interesting architectures and properties, including H_3TATB and H_3BTB (TATB denotes 4,4′,4″-s-triazine-2,4,6-triyltribenzoate and BTB denotes benzene-1,3,5-tribenzoate) [18–20]. At the same time, with its three carboxylate groups almost perpendicular to the central benzene ring, a nonplanar ligand H_3TMTA (TMTA denotes 4,4′,4″-(2,4,6-trimethylbenzene-1,3,5-triyl)tribenzoate) has also been applied to build CPs with appealing topologies [21–23].

On the other hand, thousands of CPs based on the transition metal ions have been intensively investigated. Compared with transition metal ions, there exists a kind of rare earth metal ion, which possesses abundant luminescent properties. It should be pointed out that although quite a lot of coordination complexes have been developed using different ligands in the past years, to the best of our knowledge, porous frameworks built from rigid three-tricarboxylate ligands and rare earth ions are still rare.

In the present paper, a novel rare earth complex was constructed from a rigid three-connected H_3TMTA ligand and a praseodymium(III) ion, $(Pr(TMTA)(H_2O)_2]\cdot[DMF\cdot 2EtOH\cdot 4H_2O]$ [**1**, H_3TMTA = 4,4′,4″-(2,4,6-trimethylbenzene-1,3,5-triyl)tribenzoic acid). Interestingly, complex **1** shows permanent porosity and a moderate adsorption heat of CO_2 (21.6 kJ·mol^{-1}), which can be used as a platform for the selective adsorption of CO_2/CH_4 (3.56).

2. Experimental

2.1. Materials and Methods

All chemicals were used as commercially received without further purification. The FT-IR spectra were collected from 400 to 4000 cm^{-1} using the KBr pellet method. The elemental analyses (for C, H, or N) were performed on a Perkin-Elmer 240 elemental analyzer ((PerkinElmer, Billerica, MA, USA). The powder X-ray diffraction measurements were performed with a Bruker AXS D8 Advance instrument (Karlsruhe, Germany). The thermogravimetric analysis was recorded on a Mettler Toledo instrument (Mettler Toledo, Zurich, Swiss). The gas uptake was performed on the surface area analyzer ASAP-2020 (Micromeritics, Norcross, GA, USA).

*2.2. Synthesis of [Pr(TMTA)(H_2O)$_2$]·[DMF·2EtOH·4H_2O] (**1**)*

H_3TMTA (2 mg, 0.0045 mmol) and $Pr(NO_3)_3·6H_2O$ (9.2 mg, 0.02 mmol) were dissolved in mixed solvents, DMF:EtOH:H_2O (v:v:v = 1:1:1; 1 mL). The resulting green solution was sealed in a glass tube, heated to 75 °C in 5 h, kept for 40 h, then slowly cooled to 30 °C in 8 h. The green rod crystals were collected, washed with EtOH, and dried in the air (yield: 40%). Elemental analysis calcd (%) for **1**: C 49.84, H 5.88, N 1.57; found: C 48.98, H 5.77, N 1.74%. IR (KBr): ν (cm^{-1}) = 3349 (m), 1618 (m), 1554 (s), 1419 (s), 1367 (s), 1273 (w), 1101 (w), 894 (w), 839 (m), 771 (m), 724 (s), 640 (m).

2.3. X-ray Crystallography

The single-crystal structure of the complex **1** was collected by an Agilent Xcalibur Eos Gemini diffractometer (Agilent Technologies, CA, USA) with a (Cu) X-ray Source (Cu-Kα λ = 1.54184 Å). The multi-scan program SADABS was applied to do the absorption corrections [24]. SHELXS-97 and SHELXL-97 were used to solve and refine the final structure of complex **1** by direct methods [25,26]. PLATON was used to add the symmetry of complex **1**. [27]. Table 1 contains the crystallographic details of complex **1** and Table 2 collects the selected bond lengths and angles for complex **1**.

Table 1. Crystal data for complex **1**.

Empirical Formula	**$C_{30}H_{25}O_8Pr$**
Formula weight	654.41
Temperature/K	298.15
Crystal system	monoclinic
Space group	$P2_1/n$
a/Å	9.531(3)
b/Å	16.417(5)
c/Å	27.409(8)
α/°	90.00
β/°	93.098(6)
γ/°	90.00
Volume/$Å^3$	4282(2)
Z	4
ρ_{calc}mg/mm^3	1.015
m/mm^{-1}	1.169
F(000)	1312.0
Index ranges	$-10 \leq h \leq 10, 0 \leq k \leq 18, 0 \leq l \leq 30$
Reflections collected	6198
Independent reflections	6198[R(int) = 0.1019]
Data/restraints/parameters	6198/906/354
Goodness-of-fit on F^2	1.002
Final R indexes [I >= 2σ (I)]	R_1 = 0.1012, wR_2 = 0.2613
Final R indexes [all data]	R_1 = 0.1277, wR_2 = 0.2752
Largest diff. peak/hole/e $Å^{-3}$	5.28/−1.63

Table 2. Selected bond lengths (Å) and angles (°) for complex **1**.

Pr1-O1	2.390(8)	Pr1-O1w	2.496(8)	Pr1-O2 [1]	2.384(8)
Pr1-O2w	2.488(8)	Pr1-O3 [2]	2.535(8)	Pr1-O4 [2]	2.570(8)
Pr1-O5 [3]	2.445(8)	Pr1-O6 [4]	2.480(8)	Pr1-O6 [3]	2.967(8)
O1-Pr1-O1w	77.9(3)	O1-Pr1-O2w	78.6(3)	O1-Pr1-O3 [1]	76.5(3)
O1-Pr1-O4 [1]	124.3(3)	O1-Pr1-O5 [2]	155.4(3)	O1-Pr1-O6 [2]	138.1(3)

[1] 1 − X, −Y, −Z; [2] −1/2 + X, −1/2 − Y, −1/2 + Z; [3] −1 + X, 1 + Y, +Z; [4] 1 − X, −1 − Y, −Z.

CCDC 1582391 contains the supplementary crystallographic data of complex **1** for this paper. These data could be obtained free of charge via www.ccdc.cam.ac.uk/conts/retrieving.html (or from the CCDC, 12 Union Road, Cambridge CB2 1EZ, UK; fax: +44 1223 336033; E-mail: deposit@ccdc.cam.ac.uk).

3. Results and Discussion

3.1. Crystal Structure of Complex **1**

Complex **1** was obtained in mixed solvents of DMF:EtOH:H_2O by a hydrothermal reaction of H_3TMTA and $Pr(NO_3)_3{\cdot}6H_2O$ at 75 °C. The single-crystal X-ray analysis shows that complex **1** crystalizes in a monoclinic crystal system with a p21/n space group. The asymmetry unit of complex **1** contains a praseodymium ion, a $TMTA^{3-}$ ligand, and two coordinated water molecules. The Pr-O distances are 2.384(8) Å and 2.967(8) Å, and the distances of Pr-Ow are 2.488(8) Å and 2.496(8) Å, respectively. As shown in Figure 1a, the Pr(III) ion in complex **1** adopts a nine-coordinated mode forming a distorted $\{PrO_9\}$ coordination sphere. It is interesting that the carboxylic groups in **1** adopt three different coordination modes: μ_1-η^1-η^1, μ_2-η^1-η^1, and μ_2-η^1-η^2. The carboxylic groups connect with the Pr(III) ion to form a one-dimensional infinite chain, and then the chains are linked by the $TMTA^{3-}$ ligand to construct a three-dimensional framework (Figure 1b).

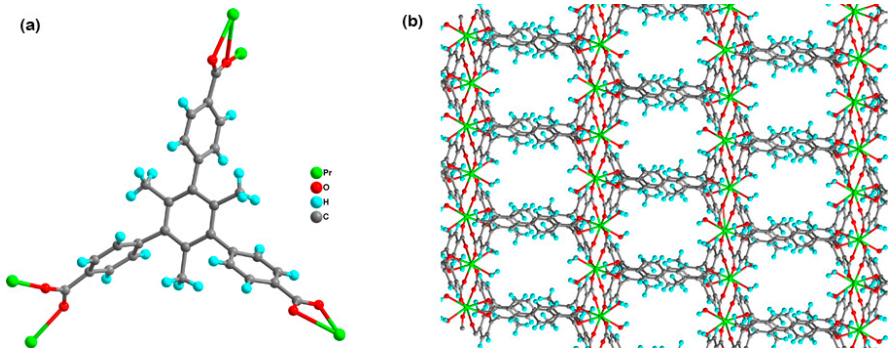

Figure 1. (**a**) View of the coordination environment around the H_3TMTA ligand and (**b**) three-dimensional porous framework of **1** viewed along the b axis.

3.2. The Fluorescent Property

Because of the presentation of rare earth ions and a rigid carboxylate group, the luminescent property of complex **1** was tested in the solid state at 298 K. The emission band centered at 362 nm (λ_{ex} = 320 nm) for H_3TMTA, which could be assigned to the electronic transition based on ligand-centered, which means the $\pi^*\rightarrow n$ or $\pi^*\rightarrow\pi$ electronic transition [28]. The emission of complex **1** was observed at 358 nm upon excitation at 320 nm for **1**, which can be attributed to the emission of H_3TMTA ligands (Figure 2). There was no characteristic emission of rare earth ions.

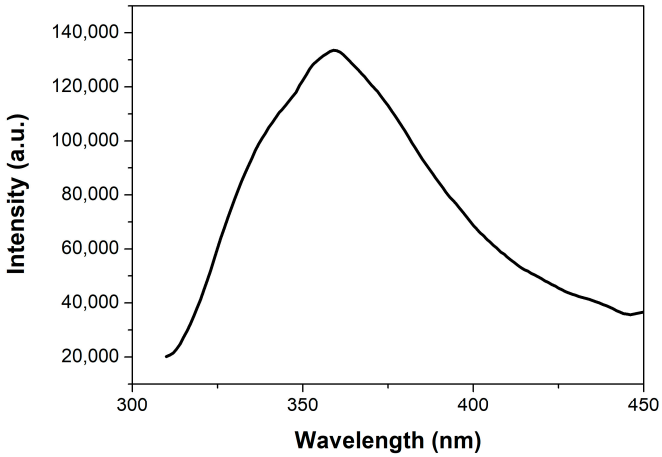

Figure 2. Solid-state fluorescence spectrum of 1 at room temperature.

3.3. Powder X-ray Diffraction Analysis

The powder X-ray diffraction pattern was used to certify the phase purity of complex **1** (Figure 3). Almost all of the peak positions of the simulated and experimental patterns match very well with each other. The preferred orientation of the powder samples accounts for the differences in intensity.

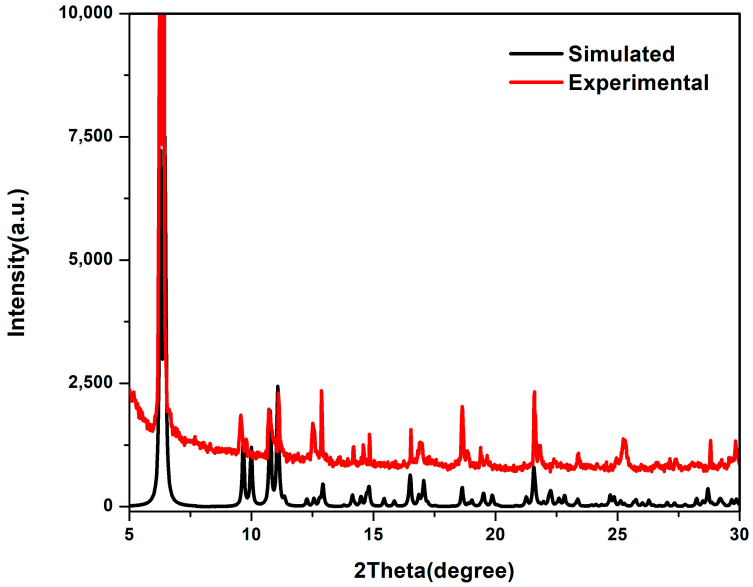

Figure 3. The powder XRD patterns and the simulated pattern from the single-crystal diffraction data for the complex **1**.

3.4. IR Spectra

The FT-IR spectrum of compound **1** was also tested. As depicted in Figure 4, the sharp bands at 1554 cm^{-1} and 1419 cm^{-1} stand for the asymmetric and symmetric stretching vibrations of the carboxylic group, respectively [29].

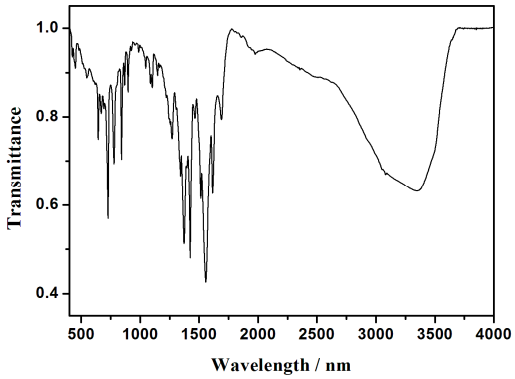

Figure 4. The IR spectra of the complex **1**.

3.5. Thermogravimetric Analyses

As shown in Figure 5, the thermogravimetric analysis (TGA) property of complex **1** was detected under an N_2 atmosphere. Complex **1** has two identifiable weight loss stages: the first stage is similar to the removal of seven uncoordinated and two coordinated solvent molecules (obsd 26.37%, calcd 27.91%), which arises between room temperature and 273 °C. The second stage belongs to the collapse of the framework, which appears at temperatures higher than 500 °C, which means that the present complex **1** shows moderate thermal stability.

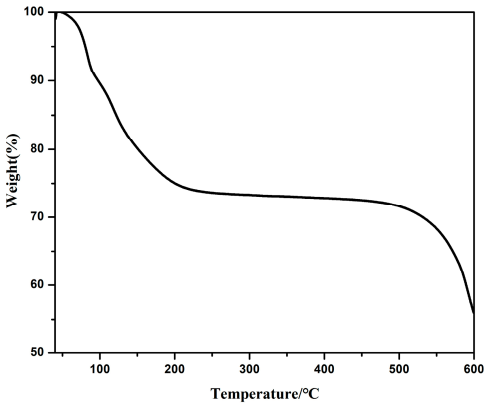

Figure 5. Thermogravimetric analysis (TGA) curves for the complex **1**.

3.6. Gas Sorption and Separation Measurements

Gas adsorption–desorption measurements of N_2, CO_2, CH_4, and H_2 on complex **1** were collected on a Micromeritics ASAP 2020 surface area and pore size analyzer at different temperatures: 77 K (liquid nitrogen bath), 273 K (ice-water bath), and 298 K (room temperature). The Brunauer-Emmett-Teller (BET) surface area and pore size distribution data were calculated from the N_2 adsorption isotherms at 77 K.

The as-synthesized crystals of complex **1** were exchanged three times with dry methanol. The activated phases samples were degassed at 353 K for 10 h for the gas sorption measurements. As can be seen from Figure 6, the active phase is highly crystalline and remains almost identical to its as-synthesized phase. The permanent porosity of complex **1** was confirmed by the reversible N_2 sorption measurements at 77 K and 1 atm, which showed a type I adsorption isotherm performance with a saturated adsorption amount of 106 $cm^3\ g^{-1}$. The values of the Brunauer-Emmett-Teller (BET) and Langmuir surface areas are 327.4 and 422.7 $m^2\ g^{-1}$, respectively, calculated from the N_2 sorption isotherm. The pore size distribution is determined with NLDFT and calculated from N_2 adsorption

isotherms at 77 K, corresponding to the pore size of 4.3 Å for complex **1**, which matches well with the crystal data.

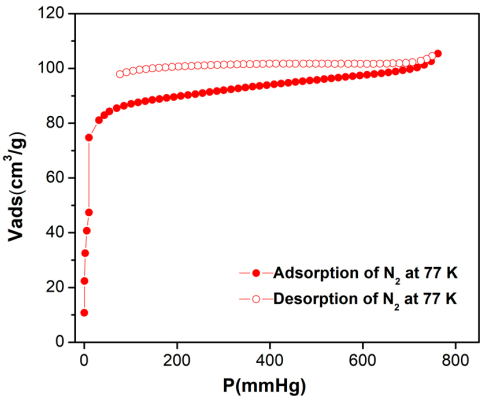

Figure 6. N_2 isotherms at 77 K for complex **1**.

We also tested the low-pressure H_2, CO_2, and CH_4 uptakes of a desolvated sample of complex **1** by using volumetric gas adsorption measurements. Complex **1** can adsorb 89.5 cm^3 g^{-1} of H_2 molecules. Thus, the CO_2 uptake of complex **1** is 26.2 $cm^3 \cdot g^{-1}$ (5.158 wt %) at 273 K and 17.6 $cm^3 \cdot g^{-1}$ (3.46 wt %) at 298 K under 1 bar, respectively (Figure 7). The adsorption heat (Q_{st}) of CO_2 of complex **1** is 21.6 $kJ \cdot mol^{-1}$ calculated from the Clausius-Clapeyron equation, indicating a moderate adsorbate-adsorbant interaction. Furthermore, the CH_4 uptake of complex **1** is 11.6 $cm^3 \cdot g^{-1}$ at 273 K and 7.5 $cm^3 \cdot g^{-1}$ at 298 K under 1 bar, respectively.

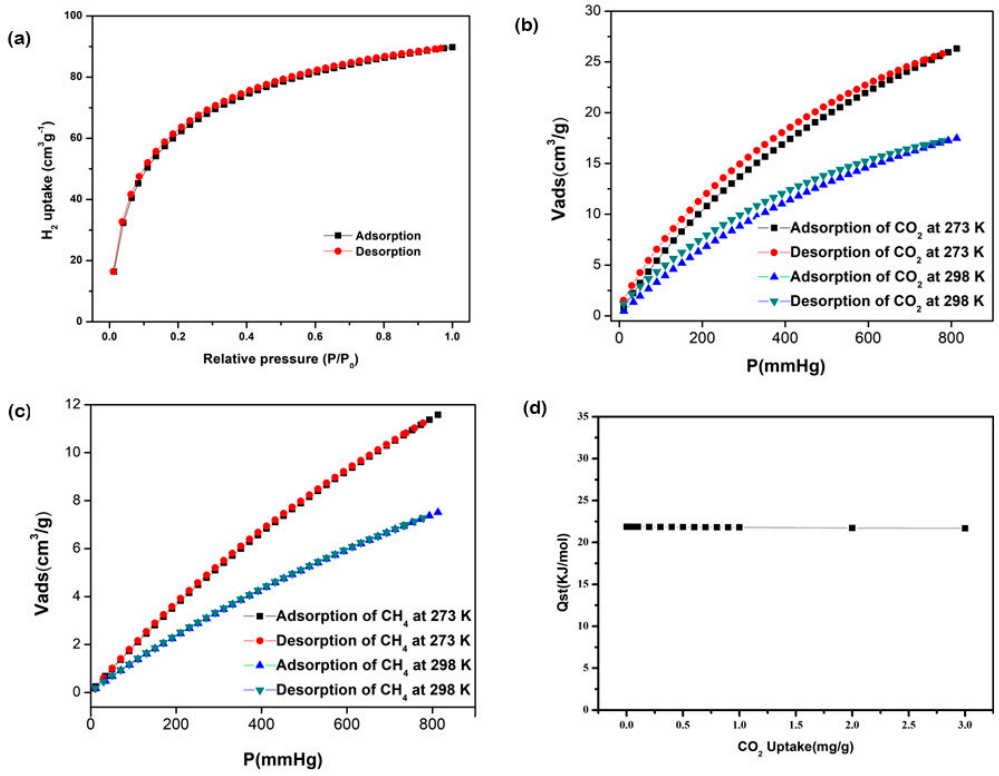

Figure 7. Gas uptakes for complex **1**. (**a**) The H_2 adsorption capacity for complex **1** at 77 K; (**b**) The CO_2 adsorption capacity for complex **1** at 273 and 298 K; (**c**) The CO_2 adsorption capacity for complex **1** at 273 K and 298 K; (**d**) The *Q*st of complex **1** for CO_2.

Since CO_2 is a dominant component of greenhouse gas and a main contaminant of natural gas, it is meaningful to investigate the capacity of CO_2 and the selectivity of CO_2/CH_4. The higher CO_2 uptake capacity of complex **1** prompted us to further investigate the selectivity of CO_2 adsorption over CH_4. According to the calculation results over a 10:90 and 50:50 CO_2/CH_4 mixed gas, the CO_2/CH_4 selectivitie at 273 K and 298 K are 3.2 and 3.56, respectively. These values are comparable to ZIF-79 (CO_2/CH_4: 5.4) [30], SIFSIX-2-Cu (CO_2/CH_4: 5.3) [31], and PCN-88 (CO_2/CH_4: 5.3) [32] (Figure 8). The results show that compound **1** may be a candidate for CO_2 capture and separation from natural gas.

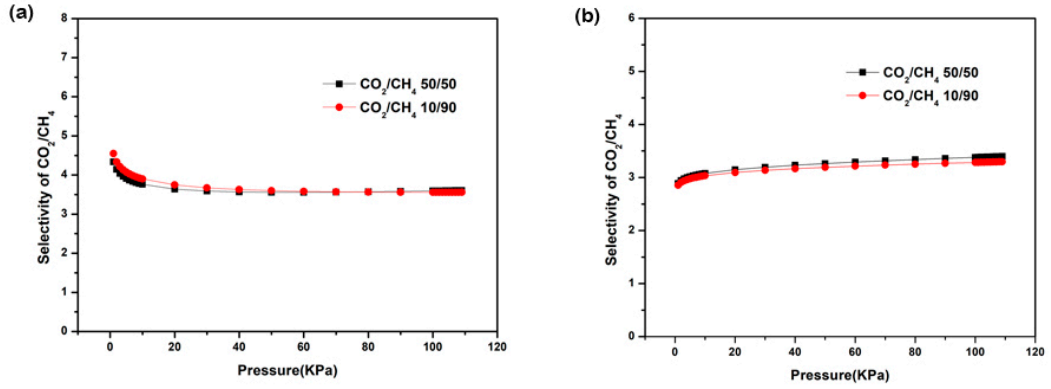

Figure 8. Selective gas adsorption for complex **1**. The CO_2/CH_4 sorption isotherms for complex **1** at 273 K (**a**) and 298 K (**b**) calculated by the IAST method for two CO_2 concentration.

4. Conclusions

In conclusion, A novel Pr complex, constructed from a rigid three-connected H_3TMTA and a praseodymium(III) ion, has been constructed under solvothermal conditions. Thus, the thermal stabilities and the fluorescent and gas adsorption and separation properties of complex **1** were investigated systematically. Complex **1** can be used as a candidate for CO_2 capture and separation from natural gas.

Acknowledgments: We gratefully thank the National Natural Science Foundation of China (No. 21401096) and Open Funds for Key Laboratory of Marine Biotechnology in Colleges and Universities of Shandong Province for the financial support.

Author Contributions: Jie Sun and Minghui Zhang designed the experiments; Aiyun Wang performed the experiments; Ziwei Cai analyzed the data and Jie Sun wrote the paper.

Conflicts of Interest: The authors declare no conflict of interest.

References

1. Forgan, R.S.; Smaldone, R.A.; Gassensmith, J.J.; Furukawa, H.; Cordes, D.B.; Li, Q.; Wilmer, C.E.; Botros, Y.Y.; Snurr, R.Q.; Slawin, A.M.Z.; et al. Nanoporous carbohydrate metal-organic frameworks. *J. Am. Chem. Soc.* **2012**, *134*, 406–417. [CrossRef] [PubMed]
2. Zheng, S.-T.; Bu, J.T.; Li, Y.; Wu, T.; Zuo, F.; Feng, P.; Bu, X. Pore space partition and charge separation in cage-within-cage indium–organic frameworks with high CO_2 uptake. *J. Am. Chem. Soc.* **2010**, *132*, 17062–17064. [CrossRef] [PubMed]
3. Bloch, E.D.; Queen, W.L.; Krishna, R.; Zadrozny, J.M.; Brown, C.M.; Long, J.R. Hydrocarbon separations in a metal-organic framework with open iron(II) coordination sites. *Science* **2012**, *335*, 1606–1610. [CrossRef] [PubMed]
4. Sumida, K.; Rogow, D.L.; Mason, J.A.; McDonald, T.M.; Bloch, E.D.; Herm, Z.R.; Bae, T.-H.; Long, J.R. Carbon dioxide capture in metal-organic frameworks. *Chem. Rev.* **2012**, *112*, 724–781. [CrossRef] [PubMed]
5. Suh, M.P.; Park, H.J.; Prasad, T.K.; Lim, D.W. Hydrogen storage in metal-organic frameworks. *Chem. Rev.* **2012**, *112*, 782–835. [CrossRef] [PubMed]

6. Li, J.R.; Sculley, J.; Zhou, H.-C. Metal-organic frameworks for separations. *Chem. Rev.* **2012**, *112*, 869–932. [CrossRef] [PubMed]
7. Yoon, M.; Srirambalaji, R.; Kim, K. Homochiral metal-organic frameworks for asymmetric heterogeneous catalysis. *Chem. Rev.* **2012**, *112*, 1196–1231. [CrossRef] [PubMed]
8. Ma, L.; Abney, C.; Lin, W. Enantioselective catalysis with homochiral metal–organic frameworks. *Chem. Soc. Rev.* **2009**, *38*, 1248–1256. [CrossRef] [PubMed]
9. Sun, D.; Ma, S.; Ke, Y.; Collins, D.J.; Zhou, H.-C. An interweaving MOF with high hydrogen uptake. *J. Am. Chem. Soc.* **2006**, *128*, 3896–3897. [CrossRef] [PubMed]
10. Ma, S.; Sun, D.; Ambrogio, M.; Fillinger, J.A.; Parkin, S.; Zhou, H.-C. Framework-catenation isomerism in metal–organic frameworks and its impact on hydrogen uptake. *J. Am. Chem. Soc.* **2007**, *129*, 1858–1859. [CrossRef] [PubMed]
11. Ma, S.; Wang, X.-S.; Yuan, D.; Zhou, H.-C. A coordinatively linked Yb metal-organic framework demonstrates high thermal stability and uncommon gas-adsorption selectivity. *Angew. Chem. Int. Ed.* **2008**, *47*, 4130–4133. [CrossRef] [PubMed]
12. Ma, S.; Yuan, D.; Wang, X.-S.; Zhou, H.-C. Microporous lanthanide metal-organic frameworks containing coordinatively linked interpenetration: Syntheses, gas adsorption studies, thermal stability analysis, and photoluminescence investigation. *Inorg. Chem.* **2009**, *48*, 2072–2077. [CrossRef] [PubMed]
13. Ma, S.; Yuan, D.; Chang, J.-S.; Zhou, H.-C. Investigation of gas adsorption performances and H_2 affinities of porous metal-organic frameworks with different entatic metal centers. *Inorg. Chem.* **2009**, *48*, 5398–5402. [CrossRef] [PubMed]
14. Chen, B.; Eddaoudi, M.; Hyde, S.T.; O'Keeffe, M.; Yaghi, O.M. Interwoven metal-organic framework on a periodic minimal surface with extra-large pores. *Science* **2001**, *291*, 1021–1023. [CrossRef] [PubMed]
15. Kim, J.; Chen, B.; Reineke, T.M.; Li, H.; Eddaoudi, M.; Moler, D.B.; O'Keeffe, M.; Yaghi, O.M. Assembly of metal–organic frameworks from large organic and inorganic secondary building units: New examples and simplifying principles for complex structures. *J. Am. Chem. Soc.* **2001**, *123*, 8239–8247. [CrossRef] [PubMed]
16. Chae, H.K.; Siberio-Perez, D.Y.; Kim, J.; Go, Y.; Eddaoudi, M.; Matzger, A.J.; O'Keeffe, M.; Yaghi, O.M. A route to high surface area, porosity and inclusion of large molecules in crystals. *Nature* **2004**, *427*, 523–527. [CrossRef] [PubMed]
17. Gedrich, K.; Senkovska, I.; Klein, N.; Stoeck, U.; Henschel, A.; Lohe, M.R.; Baburin, I.A.; Mueller, U.; Kaskel, S. A highly porous metal-organic framework with open nickel sites. *Angew. Chem. Int. Ed.* **2010**, *49*, 8489–8492. [CrossRef] [PubMed]
18. Yang, X.; Lin, X.; Zhao, Y.; Zhao, Y.; Yan, D. Lanthanide metal-organic framework microrods: Colored optical waveguides and chiral polarized emission. *Angew. Chem. Int. Ed.* **2017**, *56*, 7853–7857. [CrossRef] [PubMed]
19. Cui, Y.; Yue, Y.; Qian, G.; Chen, B. Luminescent functional metal-organic frameworks. *Chem Rev.* **2012**, *112*, 1126–1162. [CrossRef] [PubMed]
20. Feng, X.; Guo, N.; Chen, H.; Wang, H.; Yue, L.; Chen, X.; Ng, S.; Liu, X.; Ma, L.; Wang, L. A series of anionic host coordination polymers based on azoxybenzene carboxylate: Structures, luminescence and magnetic properties. *Dalton Trans.* **2017**, *46*, 14192–14200. [CrossRef] [PubMed]
21. Zhao, X.; He, H.; Dai, F.; Sun, D.; Ke, Y. Supramolecular isomerism in honeycomb metal–organic frameworks driven by CH . . . π interactions: Homochiral crystallization from an achiral ligand through chiral inducement. *Inorg. Chem.* **2010**, *49*, 8650–8652. [CrossRef] [PubMed]
22. Zhao, X.; Dou, J.; Sun, D.; Cui, P.; Sun, D.; Wu, Q. A porous metal-organic framework (MOF) with unusual 2D→3D polycatenation based on honeycomb layers. *Dalton Trans.* **2012**, *41*, 1928–1930. [CrossRef] [PubMed]
23. Zhao, X.; Liu, F.; Zhang, L.; Sun, D.; Wang, R.; Ju, Z.; Yuan, D.; Sun, D. Achieving a rare breathing behavior in a polycatenated 2D to 3D net through a pillar-ligand extension strategy. *Chem. Eur. J.* **2014**, *20*, 649–652. [CrossRef] [PubMed]
24. Bruker. *SMART, SAINT and SADABS*; Bruker AXS Inc.: Madison, WI, USA, 1998.
25. Sheldrick, G.M. *SHELXS-97; Program for X-ray Crystal Structure Determination*; University of Gottingen: Göttingen, Germany, 1997.
26. Sheldrick, G.M. *SHELXL-97; Program for X-ray Crystal Structure Refinement*; University of Gottingen: Göttingen, Germany, 1997.
27. Spek, A.L. *PLATON; A Multipurpose Crystallographic Tool*; Utrecht University: Utrecht, The Netherlands, 2002.

28. Zhang, L.; Guo, J.; Meng, Q.; Wang, R.; Sun, D. Syntheses, structures and characteristics of four metal–organic coordination polymers based on 5-hydroxyisophthalic acid and N-containing auxiliary ligands. *CrystEngComm* **2013**, *15*, 9578–9587. [CrossRef]
29. Nakamoto, K. *Infrared and Raman Spectra of Inorganic and Coordination Compounds*; John Wiley & Sons: New York, NY, USA, 1986.
30. Phan, A.; Doonan, C.J.; Uribe-Romo, F.J.; Knobler, C.B.; O'Keeffe, M.; Yaghi, O.M. Synthesis, structure, and carbon dioxide capture properties of zeolitic imidazolate frameworks. *Acc. Chem. Res.* **2010**, *43*, 58–67. [CrossRef] [PubMed]
31. Nugent, P.; Belmabkhout, Y.; Burd, S.D.; Cairns, A.J.; Luebke, R.; Forrest, K.; Pham, T.; Ma, S.; Space, B.; Wojtas, L.; et al. Porous materials with optimal adsorption thermodynamics and kinetics for CO_2 separation. *Nature* **2013**, *495*, 80–84. [CrossRef] [PubMed]
32. Li, J.R.; Yu, J.; Lu, W.; Sun, L.B.; Sculley, J.; Balbuena, P.B.; Zhou, H.C. Porous materials with pre-designed single-molecule traps for CO_2 selective adsorption. *Nat. Commun.* **2013**, *4*, 1538–1544. [CrossRef] [PubMed]